Applied Catalysis B: Environmental 193 (2016) 240–247

Contents lists available at ScienceDirect

Applied Catalysis B: Environmental

journal homepage: www.elsevier.com/locate/apcatb

Weak visible light (~mW/cm^2) organophotocatalysis for mineralization of amine, thiol and aldehyde by biphasic cobalt phthalocyanine/fullerene nanocomposites prepared by wet process

Prabhakarn Arunachalam[a,1], Shuai Zhang[a,2], Toshiyuki Abe[b], Motonori Komura[a,3], Tomokazu Iyoda[a], Keiji Nagai[a,*]

[a] Division of Integrated Molecular Engineering, Chemical Resources Laboratory, Tokyo Institute of Technology, R1-26 Suzukake-dai, Midori-ku, Yokohama 226-8503, Japan

[b] Department of Frontier Materials Chemistry, Graduate School of Science and Technology Hirosaki University, Bunkyo-cho, Hirosaki, Aomori 036-8561, Japan

ARTICLE INFO

Article history:
Received 16 July 2015
Received in revised form 7 April 2016
Accepted 14 April 2016
Available online 19 April 2016

Keywords:
Phthalocyanines
Photooxidation
Semiconductors
Cobalt
Nanoparticles
Organophotocatalyst

ABSTRACT

This article describes a visible-light-responsive photocatalyst of cobalt phthalocyanine (CoPc) and C_{60} nanocomposites synthesized by a reprecipitation process. The full-spectrum-visible-light (420–800 nm) photocatalysis was demonstrated by mineralization under illumination of weak light intensity (in the order of 1 mW/cm^2) for aqueous trimethylamine (TMA) and almost agreed with its absorption spectra. Other aqueous volatile molecules of acetaldehyde (AcH) and 2-mercaptoethanol (ME) were decomposed to CO_2. CoPc/C_{60} nanocomposite exhibited higher photocatalytic activity than independent nanoparticles of CoPc or C_{60} as well as AlPc/C_{60} composite. The oxidation power would arose from the hole generated at p/n junction like interface, which was suggested by photoelectrochemical oxidation experiments. The initial external quantum efficiencies of (EQE_{h+}) estimated from CO_2 generation reached to unity under the light intensity of 1 mW/cm^2, while later EQE_{h+} was ~10^{-4}.

1. Introduction

The photocatalytic oxidation of organic substances on a semiconductor photocatalyst is a potential method of removing organic substances from the air and water, to enable us to have comfortable and safe living [1–5]. The most extensively studied photocatalyst, TiO_2, possesses a wide band gap (e_g(anatase) ≈ 3.2 eV), which can absorb only the UV light accounting for ~4% of total sunlight to generate charge carriers for promoting surface redox reactions [1–6]. In recent years, more attention has been paid for developing new visible-light-active photocatalysts based on molecule [7–9], carbon [10–13], and inorganic solids [14–28], while only few of them are active under interior light illumination.

Organic semiconductors with heterojunctions are widely used to build low-cost and highly efficient photoenergy conversion system in dry state [29–36]. Since Tang's first report in 1986 on organic solar cell composed of Cu-phthalocyanine and a perylene derivative heterojunction bilayer [9], the field has expanded rapidly and is used to construct high-efficiency photoenergy conversion systems in the dry state. On the contrary, primary attempts of organic semiconductor as photoelectrode started more than 30 years ago [37,38]. Oligo *p*-phenylene polymer was used as a sensitizer for photoreduction of not only water molecule to H_2 [39–42] but also CO_2 to CO in the presence of triethylamine (TEA) as a sacrificial electron donor under UV (λ > 290 nm) irradiation.

Apart from the two research trends, photoelectrochemical catalysis has been used for organic *p-n* junction such as a perylene derivative (3,4,9,10-perylenetetracarboxyl-bisbenzimidazole, PTCBI) or fullerene (C_{60}) and metal-free Pc's (H_2Pc) [43–55], rr-P3HT:PCBM and so forth [56] in the water phase, wherein the evolution of O_2 from the water was found to occur along with hole conduction through the p-type layer under visible-light irradiation [44,57], while the evolution of H_2 from the water was also found with electron conduction through the n-type layer [45,47]. Organic *p-n* bilayer undergoes photoinduced redox reaction at the

* Corresponding author.
E-mail address: nagai.k.ae@m.titech.ac.jp (K. Nagai).
[1] Present address: Department of Chemistry, College of Science, King Saud University, P.O. Box 2455, Riyadh 11451, Saudi Arabia.
[2] Present address: School of Materials and Engineering, Changzhou University, Changzhou, Jiangsu 213164, PR China.
[3] Present address: Department of Electrical and Electronics Engineering, Numazu National College of Technology, 3600 Ooka, Numazu, Shizuoka 410-8501, Japan.

http://dx.doi.org/10.1016/j.apcatb.2016.04.027
0926-3373/

solid/water interface along with photophysical events (i.e. light absorption, charge separation at the *p-n* interface, and carrier conduction) in its interior. Moreover, bilayer leads to an efficient carrier generation in comparison with the single layers of Schottky junction [58,59]. An example of the carrier generation without contact electrode is laser-induced reflection for infrared light happened by the photogenerated free electrons in perylene derivative (PTCBI) [60,61].

A visible-light-responsive photocatalyst comprising only organic material based on *p-n* junction has termed to be organophotocatalyst [62,63]. We fabricated an organophotocatalyst composed of a perylene derivative and H_2Pc coated onto a Nafion membrane by the dry process for the photoxidation of trimethylamine (TMA). However, considering the high cost of a dry process (i.e., vapor deposition), it is essential to find an alternative process. A kind of wet process of a reprecipitation from a polar solvent gave biphasic nanocrystals of aluminum phthalocyanine (AlPc) and fullerene [53,64,65], while previous reprecipitation invented by Kasai et al. gave a single component of organic crystals though whose size is controllable between nanometers to micrometers [66–68]. The choice of N-methyl-2-pyrrolidone (NMP) [69] as a polar good solvent [53,64] is crucial issue not to form single phase crystal of charge transfer (CT) complex based on electron donor-acceptor interaction, while such single phase D-A complex was obtained by the choice of non-polar good solvent such as toluene for porphyrin-C_{60} combination [70–73].

Cobalt phthalocyanine (CoPc) is interesting from the view point of oxidation catalysis [74–82], then is expected to be efficient hole consumption. In this study, we will report the synthesis and photocatalytic properties of biphasic nanoparticles comprised of CoPc and fullerene. The photocatalysis properties are evaluated in terms of mineralization of trimethylamine, 2-mercaptoethanol and acetaldehyde to CO_2 under visible-light irradiation (in the order of <1 mW/cm^2).

2. Materials and methods

2.1. Materials

C_{60} (99%) was obtained from Tokyo Chemical Industry Co., Ltd. (TCI) and used as received. CoPc (TCI) was purified twice by sublimation prior to use. Glass substances with ITO coating of 174 nm thickness were commercially available from Asahi Glass Co., Ltd., and were washed by sonication in water-containing detergent, acetone, and ethanol in this sequence. The plates were dried in the air finally before use.

2.2. Synthesis

The C_{60}, CoPc or composite nanoparticles were prepared by dissolving 20 mg of C_{60}, and/or CoPc in 40 mL of NMP as a good solvent. This solution was then injected into 400 mL water by a syringe pump with an injection rate of 5 mL/min. During the injection, the mixture was vigorously agitated with a rate of 700 rpm, which was kept after the injection for 30 min to form a suspension. When the nanoparticles were collected by filtration, 1% (volume ratio) of 1 M HCl was added to the suspension, and the mixture was kept overnight to aggregate the nanocrystals. The particles were collected by filtration (hydrophilic PTFE membrane, pore size 0.2 μm), in which NMP and HCl were removed by gently washing with water 3 times. The nanoparticles were thoroughly washed with distilled water and kept in a deep freezer (−45 °C) for 2 h. Then the frozen nanoparticles were dried with a vacuum of 100 Pa at −10 °C.

2.3. Characterization

UV–vis absorption spectra were recorded using Shimadzu UV-3100S. Transmission electron microscopy (TEM) images were obtained by applying a drop of dilute particle suspension to a carbon-coated copper grid, and they were recorded with Hitachi H-7100. X-ray powder diffraction (XRD) measurements were performed on a Rigaku Rint Ultima+ diffractometer using Cu Kα irradiation. The size distribution of nanoparticles suspension was determined by dynamic light scattering (DLS) using the Malvern Zetasizer Nano ZS at 25 °C. The parameters for the analysis of NMP/water mixture refraction index and the viscosity of the NMP/water are 13.5 and 9.6 Pa s, respectively.

2.4. Photocatalytic oxidation

The photocatalytic oxidation of TMA, 2-mercaptoethanol (ME) or acetaldehyde (AcH) was tested. In a cylindrical Pyrex cell (2 mL), 0.08 mg of the nanoparticles and the aqueous substance (0.4 mL, 1 wt%) was placed. The reactor was irradiated with visible light emitted by a 150-W halogen lamp with an interference filter and a cutoff filter for IR Light. The photon number of almost monochromatic light (FWHM ~ 10 nm) was 3.5×10^{13} cm^{-2} s^{-1} (@1 mW/cm^2 for 600 nm) which was monitored and adjusted by optical power meter. The irradiation area was 1 cm^2. The amount of CO_2 generated was detected by a GC–MS (GC; Agilent 7890A. MS; JEOL-JMT-QT400GCP) equipped with a porapak Q column.

2.5. Reusabilty test

The reusability of the prepared composite nanoparticles was tested by repeating the several cycles of photocatalytic oxidation of AcH. After every cycle, organic substance was removed by argon purging, and fresh AcH was injected into the cell.

2.6. Visible light inorganic photocatalyst test

Splay type WO_3 particles were purchased from Toshiba Lightech (Rene WO_3), and splayed to a sample tube and dried.

3. Results and discussion

3.1. Characterization of particles

The absorption spectra of C_{60}, CoPc and their mixture solutions in NMP are shown in Fig. 1A. The spectrum of C_{60} (dot line a) exhibited a characteristic shoulder at 340 nm [69], and that of CoPc solution (broken line b) had Q-band absorption with a peak at 675 nm [79]. For the mixture solution of C_{60} and CoPc (dashed line c), absorption band did not show shift or intensity change compared to the arithmetic sum of two mono-component spectra (solid line d). This indicates that no significant interaction has occurred between C_{60} and CoPc in the NMP solution as a polar solvent. This observation contrasts with the report on porphyrin/fullerene complex in toluene as a non-polar solvent where a charge transfer band appears at 650–800 nm [70–73].

The reprecipitation process gave nanoparticle suspension. As for the suspension from the mixed solution of C_{60} and CoPc, composite **c** and **d** denote the nanoparticles of mixing ratios of C_{60}/CoPc = 1/1 and C_{60}/CoPc = 2/1, (wt/wt) respectively. The molar ratios were estimated to be 0.86/1.0 for composite **c** and 1.85/1.0 for composite **d** from elemental analysis (Table S1), while excess H_2O remained. In each of C_{60}, CoPc, and composite **c**, the absorption band of the suspension (lines a–c in Fig. 1B) was broader than that of the corresponding NMP solution (lines a–c in Fig. 1A). This broadening agrees with solidification to be nanoparticle in NMP/water (1/10 = v/v)

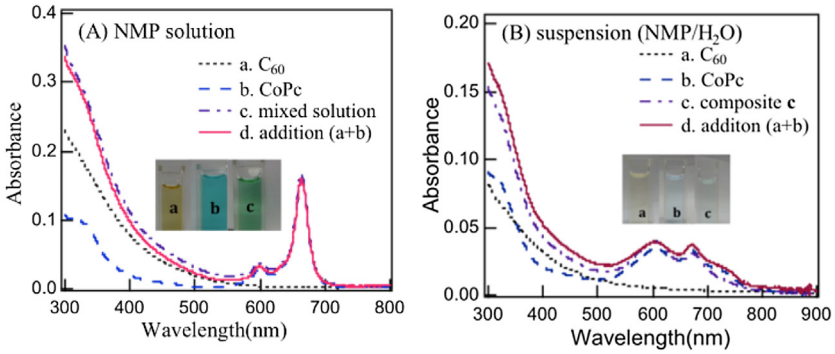

Fig. 1. UV–vis absorption spectra of (a) a. C_{60} (4.3×10^{-3} mg/mL), b. CoPc (4.3×10^{-3} mg/mL) c. mixture of CoPc and C_{60} in NMP solution (8.6×10^{-3} mg/mL), and d. arithmetic addition of the spectra (a + b). (b) Absorption spectra of particle suspension of a. C_{60} particle suspension (8.6×10^{-4} mg/mL), b. CoPc particle suspension (8.6×10^{-4} mg/mL), c. composite particle suspension (1.72×10^{-3} mg/mL) and d. arithmetic addition of the spectra (a + b). The broadenings in suspension in comparison with NMP spectra are indicative of nanoparticle formation in NMP/water suspension medium.

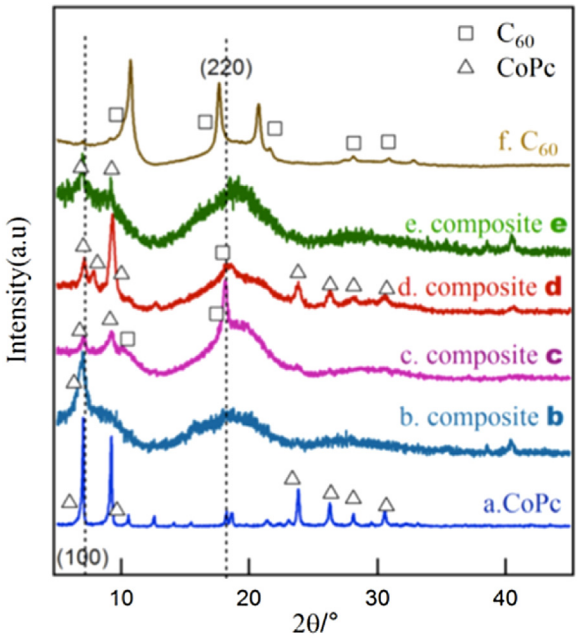

Fig. 2. Normalized XRD spectra of a. CoPc, b. composite **b**, c. composite **c**, d. composite **d**, e. composite **e**, and f. C_{60} nanoparticles. The peaks from C_{60} and CoPc are marked with rectangles and triangles, respectively. The freeze drying process was employed to get powder form of nanoparticles. The composite retains the diffraction peak of C_{60} and CoPc, indicating the biphasic behavior of nanoparticles.

medium [86], and is similar to the case of AlPcCl/C_{60} nanoparticles [53]. In addition, the absorption spectrum of composite (line c in Fig. 1B) was similar to the sum of the absorption spectra of CoPc and C_{60} suspensions, and implies that composite particle contains of both C_{60} and CoPc nanoparticles.

Fig. 2 depicts the XRD patterns of C_{60}, CoPc and their composites of C_{60} and CoPc. The composite with a feeding ratio of C_{60}/CoPc = 1/4 is denoted as composite **b**, and a ratio of 1/0.25 is denoted as composite **e**. The CoPc single component particles exhibited the peak at 7.0°, 9.2°, 10.6°, 12.5°, 15.4°, 18.2°, 23.1°,23.8°, 26.2° and 28.2° (line a in Fig. 2) indexed as the (100), (102), (002), (202), (102), (104), (290), (112), (311) and (106) planes of the β phase of CoPc crystal [83]. C_{60} particles showed (line f in Fig. 2) peaks at 2θ = 10.9°, 16.9°, 20.6°, 29.4°, 27.4° and 28.1° indexed as the (111), (220), (311), (222), (331) and (420) planes of the face-centered-cubic pristine [84]. All of composites exhibited sharp peak at 7.0°, which is characterized to be (100) plane of CoPc, in spite of broadening of other peaks except composite **d**. On the other hand, the peaks of C_{60} were broadened and only the peak at 18° was clearly observed. These peaks characterized to CoPc and C_{60} implies biphasic structure of CoPc/C_{60} composite and smaller crystalline size than CoPc or C_{60} monocomponent nanocrystals.

Table 1
Particle size of nanoparticles.

	TEM[a] (nm)	DLS[b] (nm)	XRD[c] (nm)
C_{60}	38 ± 2	41 ± 2	17
CoPc	78 ± 5	91 ± 5	29
Composite **c** CoPc/C_{60}	42 ± 2	36 ± 2	38
Composite **d** CoPc/C_{60}	32 ± 2	28 ± 2	15
Composite C_{60}/AlPcCl[d]	–	57 ± 2	–

[a] Particle size measured from TEM images by considering 100 particles.
[b] Obtained from dynamic light scattering (DLS) measurements of the nanoparticle.
[c] Determined from XRD pattern using Scherer equation.
[d] The composite particle prepared through the precipitation process from AlPcCl and C_{60} [64].

TEM images of the C_{60} and CoPc nanoparticles reveal particle size. From them, the histograms of particle size are shown in Fig. 3. These size range are from 7 to 80 nm for C_{60} (Fig. 3a) and 25–110 nm for CoPc (Fig. 3b). For nanoparticles of **c** and **d**, the sizes are of 10–110 nm and 10–80 nm, respectively. The average particle sizes for C_{60}, CoPc and composite **c** and composite **d** are estimated from Fig. 3 and shown in Table 1a.

The particle sizes of nanoparticles obtained from dynamic light scattering (DLS) methods are shown in Fig. S1. The average sizes are consistent with the particle size observed by TEM. The particle sizes are also estimated from the XRD pattern using Scherer equation [85] for the C_{60}, CoPc and composite particles **c** and **d** as shown in Table 1. The average particle sizes of the nanoparticles evaluated from XRD were smaller than those from TEM and DLS, and this tendency was similar to the case of AlPc and AlPc/C_{60} [53,64].

For all observation of TEM, DLS, and XRD, the composite of CoPc/C_{60} showed smaller size than mono component CoPc or C_{60}. The smaller size would be faster nucleation formation due to weak interaction between CoPc or C_{60} in the Water/NMP mixture.

3.2. Photoelectrochamistry

It is very difficult to characterize p/n junction formation in a particle. The discussion based on photoelectrochemisty is useful. The cyclic voltammograms show characteristic photoanodic current for single layer and bilayer electrodes prepared by vapor deposition (well characterized *p-n* junction for bilayer). As shown in Fig. S2, the vapor deposited ITO/C_{60}/CoPc electrode also showed superior photoanodic current (Fig. S2c), while the inversed layering of

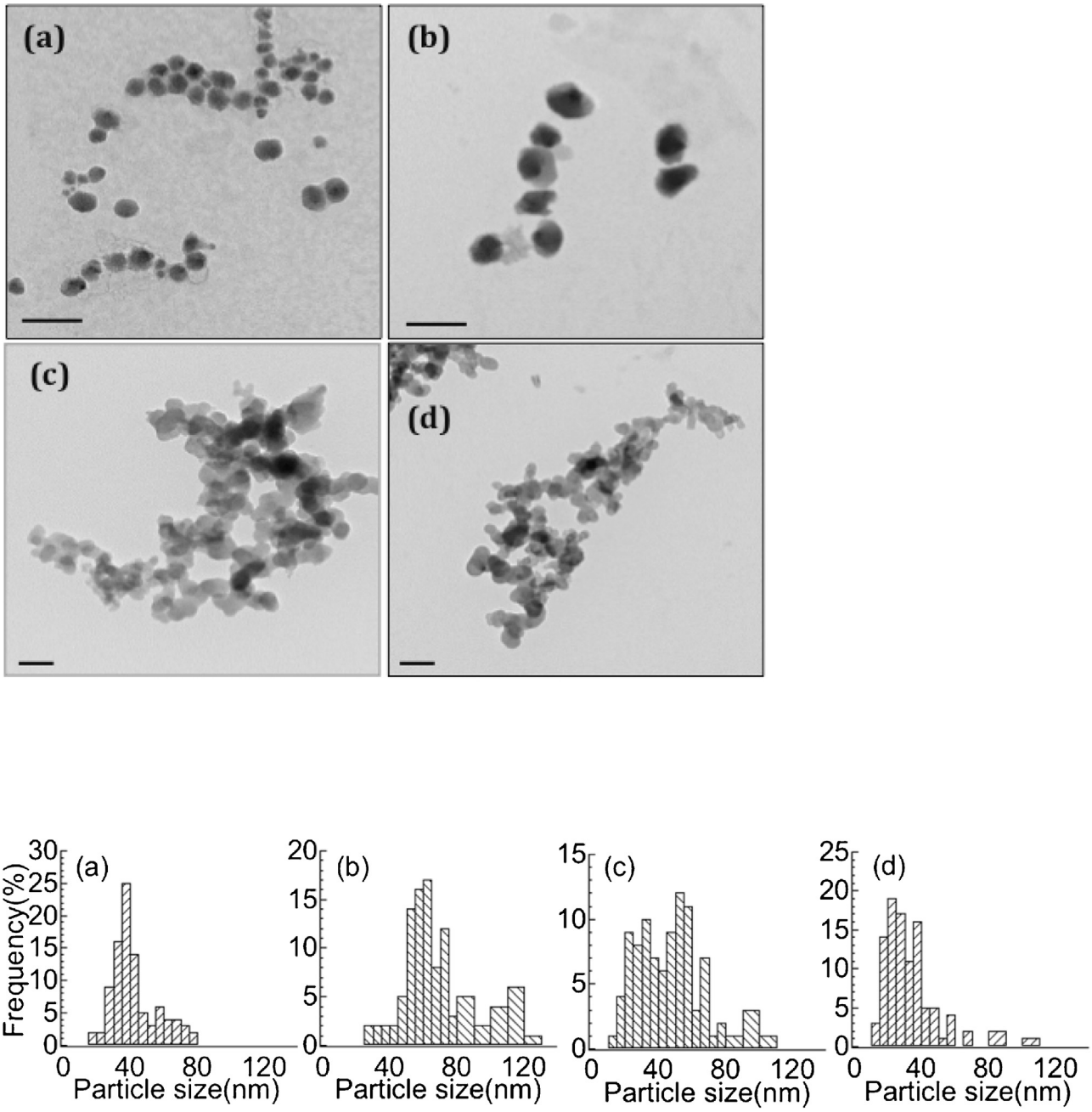

Fig. 3. Transmission electron microscopy (TEM) images of C_{60} (a), CoPc (b), composite **c** (c), and composite **d** (d) nanoparticles. The length of scale bars is 100 nm. The histograms of the particle size (below) were obtained by measuring 100 particles size of the sample.

ITO/CoPc/C_{60} electrode exhibited smaller photoanodic current than single layer of C_{60}.

Similarly, composite **c** and **d** nanoparticles electrode showed higher photoanodic current than C_{60} nanoparticles (Fig. S3). These can be interpreted to be contribution from particles of partially existing ITO/n/p aligned on the ITO electrode. It does not deny the existence of single component particle on ITO (ITO/p, ITO/n) and inversely aligned particles (ITO/p/n).

3.3. Photocatalytic activity

The previous reports revealed the CoPc works as autoxidation molecular catalyst of aldehyde [75], sulphide [76], indole [77], and thiol [78–81] in homogeneous medium. For example, water soluble CoPc in the presence of the base is active for thiol oxidation to a disulphide [80,81]. In order to investigate similar dark catalysis, the heterogeneous reaction in the presence of the CoPc nanocrystal was studied for aqueous phase. As shown in Table 2, CoPc nanoparticles does not show activity in the dark condition, the value of organic substance oxidation to CO_2 is <0.001 μmol, which is just above the detection limit.

The photocatalytic activities over the present nanoparticles for water phase oxidation of visible-light transparent substances such as trimethylamine (TMA), 2-mercaptoethanol (ME), and acetaldehyde (AcH) have been measured under visible-light irradiation. For comparison purpose, similar experiments are carried out for C_{60}, CoPc, and for previously reported AlPcCl/C_{60} nanoparticles [64]. A blank experiment in the absence of irradiation, but with the catalysts demonstrated that no significant amount of CO_2 was found. The composite **d** nanoparticles showed the largest CO_2

Table 2
CO_2 generation for different particle suspensions ($\times 10^{-7}$ mol).

Substance/Conditions	CoPc	C_{60}	composite **c**	composite **d**	C_{60}/AlPcCl[b]
TMA/light[a]	0.14	0.31	0.83	1.3	0.56
ME/light[a]	<0.01	0.01	0.09	0.26	0.18
AcH/light[a]	0.04	0.08	0.30	0.38	–[c]
No substance/light[a]	–[c]	–[c]	–[c]	0.05	–[c]
TMA/dark	<0.01	<0.01	<0.01	<0.01	<0.01
ME/dark	<0.01	<0.01	<0.01	<0.01	<0.01
AcH/dark	<0.01	<0.01	<0.01	<0.01	<0.01

[a] 1 wt% TMA, ME, and AcH under monochromatic light irradiation (1×10^{-3} W/cm^2) for 2 h, λ = 600 nm; 0.4 mL of 0.4 mg/ml particle suspensions.
[b] The composite particle prepared through the precipitation process from AlPcCl and C_{60} [64].
[c] No experimental data.

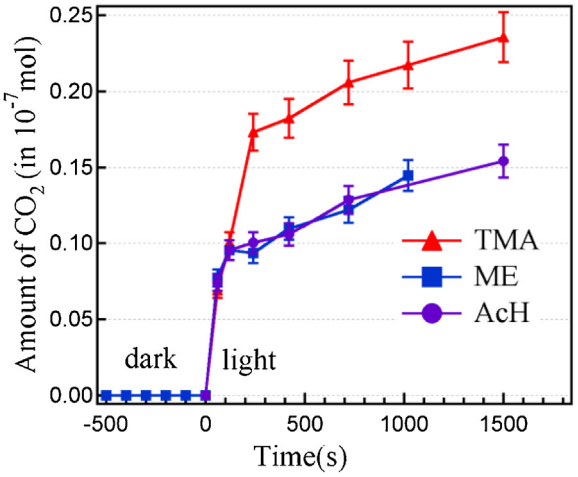

Fig. 4. Time course of CO_2 evolution from TMA, ME, and AcH decomposition under illumination on composite **d** nanoparticles. Concentration of TMA-3 wt%; ME and AcH-1 wt%; 1 mW/cm^2 was used as the light intensity (λ = 600 nm). At shorter periods kinetics are dominated by carrier generation, but at longer time intervals, kinetics of the reactions are dominated by the mass transfer of the reactants.

generation among samples of C_{60}, CoPc, composite **c**, composite **d** and AlPcCl/C_{60} nanoparticles under visible-light irradiation for 2 h (Table 2). The amount of CO_2 generated under irradiation follows the descending order of composite **d** > composite **c** > C_{60} > CoPc. This tendency was the same as the case of AlPc/C_{60} composite > C_{60} > AlPc. The superior photocatalysis of C_{60}/AlPc interface was attributed to the photogenerated hole at p/n junction [53]. Furthermore, the photocatalytic oxidation of organic substances indicates that CoPc/C_{60} (composites **c** and **d**) nanoparticles exhibited superior photocatalytic activity in comparison with AlPc/C_{60} composite nanoparticles (Table 2). Because the composite **d** showed a superior photocatalytic activity than composite **c**, we focus on the composite **d** below.

3.4. Kinetics of the photocatalysis of composite nanoparticles

The time course of the photocatalysis of oxidation were tested at the concentration of 1 wt% organic substances at the monochromatic light intensity of 1 mW/cm^2 (λ = 600 nm) as shown in Fig. 4. Control experiments under inert gas (Ar) showed much smaller increase of CO_2 shown in Fig. S4.

If the generated hole at p/n junction was consumed by oxidation, the following reactions are possible for the CO_2 generation. As a typical example, the time course of CO_2 generation for composite **d** nanoparticles shown in Fig. 4. CO_2 generation would be based on the following reactions.

$$(CH_3)_3N + 6H_2O + 21\,h^+ \xrightarrow{h\nu} 3CO_2 + 21H^+ + 1/2N_2. \quad (1)$$

$$HOCH_2CH_2SH + 5H_2O + 16\,h^+ \xrightarrow{h\nu} 2CO_2 + 16H^+ + SO_2 \quad (2)$$

$$CH_3CHO + 3H_2O + 10\,h^+ \xrightarrow{h\nu} 2CO_2 + 10H^+ \quad (3)$$

Initially, <100 s, the amount of CO_2 generated increased linearly with the time, while in the longer periods, gradual increase in the CO_2 generation was observed. Note that control experiments in the absence substance (TME, ME, or AcH) did not show considerable CO_2 increase under illumination (Table 2, no substance). Then the desorption of adsorbed of CO_2 on nanoparticles is not dominant, and initial CO_2 generation can be due to oxidation of adsorbed substance controlled by the carrier generation process, while the later CO_2 generation can be kinetically dominated by the mass transfer of the reactants.

3.5. External quantum efficiency (EQE)

The difference can be interpreted to be the change of the rate determining process as follows. In order to discuss the kinetics, for both the initial and later slopes, the photocatalysis of composite **d** nanoparticles to carbon dioxide was evaluated as external quantum efficiency (EQE) was appropriately evaluated in Eq. (4),

$$EQE = nM_{CO_2}N_A/(TIS\tau/E_{h\nu}) \quad (4)$$

where M_{CO_2}, N_A, n, I, S, τ, and $E_{h\nu}$ represent the molar number of generated CO_2 (mol), Avogadro's number, number of consumed holes for TMA oxidation (n = 1 in the present case), incident light intensity (W/cm^2), irradiation area (cm^2), irradiation time, and photon energy (J), respectively. The number of T corresponds to the number of CO_2 molecules generated from one molecule of chemical substances to be 3, 2, and 2 for TMA, ME, and AcH, respectively, as shown in Eqs. (1)–(3), which mean that all of the CO_2 generation was done by photogenerated hole at the *p-n* junction. Then the EQE denoted here as EQE_{Tnh+} (totally oxidized by photogenerated hole), when the n values are assumed to be 21, 16, and 10 for TMA, ME and AcH, respectively, according to Eqs. (1)–(3).

The EQE_{Tnh+} values for the initial and later slopes are summarized in Table 3. The initial EQE_{Tnh+} values are higher than unity, implying the existence of autoxidation. Similar high EQE_{Tnh+} values were observed in photocatalysis of volatile organic compounds not only for organophotocatalyst [62,63] but also inorganic photocatalysis [3].

In order to overcome the problem, EQE_{h+} values will be assumed for the one hole oxidation and designated as EQE_{h+}. The most conservative estimation of EQE taken autoxidation account is based on the following equation, for example, one hole is consumed in TMA oxidation to TMA^+ (Eq. (5)), and TMA^+ is autoxidized to three CO_2 molecules.

$$(CH_3)_3N \xrightarrow{h\nu} (CH_3)_3N^+ \xrightarrow{O_2} CO_2 \quad (5)$$

In the case, n value in Eq. (1) is unity and the EQE is denoted as EQE_{h+} (one hole oxidation yield). The EQE_{h+} values are estimated

Table 3
Turnover number and efficiency for the catalysis by the composite **d**.[a]

substance	EQE_{Th+} (<60 s)	EQE_{Th+} (>100 s)	EQE_{h+} (<60 s)	EQE_{h+} (>100 s)	TON (2 h)
TMA	16	7.5×10^{-3}	0.76	3.6×10^{-4}	8.4
ME	18	8.5×10^{-3}	1.1	5.3×10^{-4}	1.8
AcH	12	5.3×10^{-3}	1.2	5.3×10^{-4}	2.5

[a] 3 wt% TMA, ME, AcH; monochromatic light irradiation (1×10^{-3} W/cm^2), λ = 600 nm; 0.4 mL of 0.4 mg/ml particle suspensions.

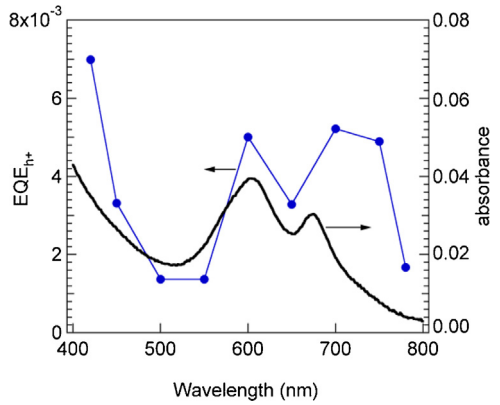

Fig. 5. EQE action spectrum for CO_2 generation from TMA decomposition calculated from Eq. (4) where n = 1 based on Eq. (5) and UV–vis absorption spectrum of composite **d** suspension (solid line). The reactors contained 0.4 mL of aqueous TMA (3 wt%) and composite **d** (0.4 mg/ml), light irradiation time of 2 h. The incident photon number intensity was adjusted to c.a. 3.5×10^{13} cm^{-2} s^{-1} at each wavelength (1×10^{-3} W cm^{-2} @550 nm). The amount of CO_2 generated from composite **d** nanoparticles are responsive to the full spectrum of visible light.

to be 0.76–1.2. Such high EQE close to unity would imply not only high hole generation yield but also high autoxidation rates to CO_2. On the other hand, later EQE than 100 s were much lower than the initial EQE for both EQE_{th+} and EQE_{h+}. These would be dominated by the mass transfer of the reactants as described before.

3.6. Wavelength dependence of the photocatalysis

The action spectrum evaluated from the TMA oxidation to CO_2 (Fig. 5). The EQE_{h+} results agree with the absorption spectra of CoPc/C_{60} for 520–800 nm, showing that the present CO_2 generations are responsive to the full spectrum of visible light. The higher EQE_{h+} than that in Table 3 would be due to the low light intensity [52]. The action spectrum matches with the sum of C_{60} and CoPc light absorption and suggesting that the exciton generation is contributed from both C_{60} and CoPc.

There can be deny a double excitation like z-scheme as recent visible light responsive photocatalyst, because if so, monochromatic light > 650 nm cannot induce photocatalysis due to no light absorption of C_{60}, and only CoPc is excited.

3.7. Repetitive use of the photocatalyst

In order to check the stability of the fabricated composite as a photocatalyst, the reusability was investigated. As a representative sample, composite **d** nanoparticles for AcH oxidation was studied under 1 mW/cm^2 illumination. It was reused for another 4 runs of the catalyst under the same condition. It was confirmed that the high photocatalytic activity retained the same as the first run and the results are shown in Fig. 6a. These results clearly showed that the composite **d** nanoparticles with high activity and stability are successfully prepared by the reprecipitation method. The stability of the composite nanoparticles was studied by comparing their absorption spectrum before and after visible-light irradiation as shown in Fig. 6b. It shows that the absorption spectrum after 48 h light irradiation is almost the same with that before light irradiation, demonstrating that the composite nanoparticles are stable under visible-light. The similar experiment was carried out at 1 mW/cm^2 illumination condition of 600 nm, similar behavior was observed. This explains that the CoPc/C_{60} nanoparticles were stable under illumination condition.

3.8. Comparison with visible light inorganic photocatalysts

As comparison experiments, WO_3 was tested as similarly (~1 mW/cm^2) as summarized in Table 4. Both the commercial WO_3 exhibited similar band gap to that reported for bare WO_3 (~2.7 eV) [21,22] (Fig. S5). For the 420 nm light illumination, the composite **d** and the WO_3 showed similar CO_2 generation. On the other hand, 600 nm light illumination for the composite **d** gave CO_2 as 4 times as that of WO_3. The present composite **d** indeed may serve as an

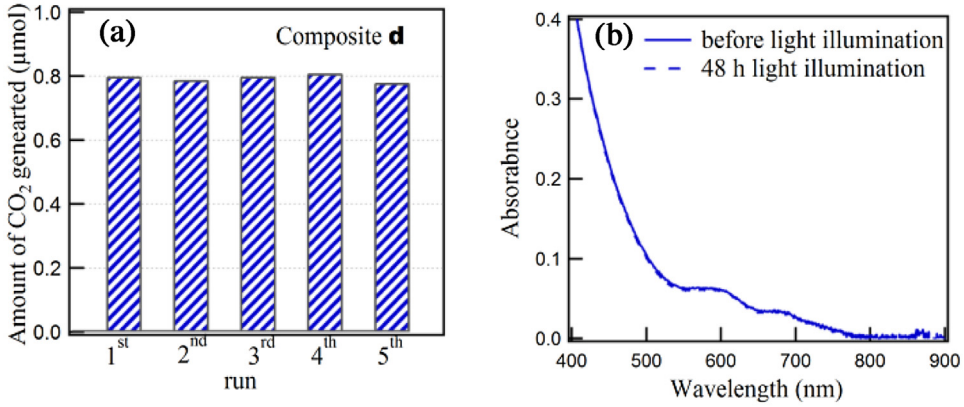

Fig. 6. (a) The amount of CO_2 generated for composite **d** nanoparticles during the several runs of the photocatalytic oxidation of acetaldehyde under visible light illumination for 1 h (1 mW/cm^2; 600 nm). In each run, 3 mL of aqueous AcH (0.05 wt%) was mixed with the composite **d** (1.2 mg) in the 15 mL pyrex cell. The amount CO_2 generation remains almost the same in all runs of the oxidation reaction. (b) Absorption spectra of composite **d** nanoparticles suspension before and after visible-light irradiation of 10 mW/cm^2 for 48 h. No changes in the absorption spectra of the nanoparticles before and after irradiation.

Table 4
Photocatalytic CO_2 generation from acetaldehyde using CoPc/C_{60} composite **d** and WO_3, depending on the light intensity and wavelength. 1.2 mg of photocatatalyst was set in a pyrex tube and 0.05% of aqueous AcH was illuminated for 1 h.

Photocatalyst	light wavelength (nm)	light intensity (mW/cm^2)	amount of CO_2 generated ($\times 10^{-6}$ mol)
composite **d**	420	1.0	1.2
composite **d**	600	1.0	0.8
composite **d**	600	0.35	0.31
composite **d**	600	3.5	2.3
WO_3	420	1.0	1.2
WO_3	600	1.0	0.19

effective photocatalyst in the photoxidation of organic substances at indoor conditions.

3.9. Turnover number

In order to confirm photocatalytic CO_2 evolution, turn over number (TON) per active site and per unit time. The TON value is determined from Eq. (6).

$$TON_{CO_2} = a/b \quad (6)$$

$$b = T_w/M_w \quad (7)$$

where a [mol] is the amount of CO_2 produced per min and b [mol] is the number of CoPc molecules, Mw is the average molecular weight of the composite **d** (668, shown in Table S1).

In the present paper, the photocatalysis was mainly studied at low light intensity. In such condition, TON is small because the reaction rate depends on light intensity. We can show a case of TON > 1 to be 1.20 in Table 4 for the AcH mineralization by composite **d** under 600 nm, 3.5 mW/cm^2 illumination.

4. Conclusion

We have investigated the photocatalytic properties of a nanoparticle composite composed of C_{60} and CoPc prepared by a reprecipitation process. The photocatalyst is having a biphasic structure. The photocatalytic results indicate that the composite C_{60}/CoPc nanoparticles catalyzed oxidation of various organic substances (TMA, ME, and AcH) using only visible light. The autoxidation behavior of organic substances on CoPc/C_{60} composite nanoparticles was implied in EQE_{h+} evaluations. The photocatalytic activity was superior for CoPc/C_{60} than that for AlPc/C_{60}. These catalysts are active at a low level of illumination (in the order of 1 mW/cm^2) and can be used for interior lighting applications. The initial reaction rate was higher than latter (>100 s) one which implied the mass transfer of the reactants and improvement by reactants condensation in the future.

Acknowledgements

A part of the work was supported by KAKENHI 26410251 from the Japan Society for the Promotion of Science. We thank Mrs. Y. Akimoto and Mrs. K. Hashimoto for technical assistance.

Appendix A. Supplementary data

Supplementary data associated with this article can be found, in the online version, at http://dx.doi.org/10.1016/j.apcatb.2016.04.027.

References

[1] N. Negishi, T. Iyoda, K. Hashimoto, A. Fujishima, Chem. Lett. 106 (1995) 841–842.
[2] Y. Kikuchi, K. Sunada, T. Iyoda, K. Hashimoto, A. Fujishima, J. Photochem. Photobiol. A: Chem. 106 (1997) 51–56.
[3] I. Sopyan, M. Watanabe, S. Murasawa, K. Hashimoto, A. Fujishima, J. Photochem. Photobiol. A Photochem. 98 (1996) 79–86.
[4] K. Hashimoto, H. Irie, A. Fujishima, Jpn. J. Appl. Phys. 44 (2005) 8269–8285.
[5] A. Fujishima, T.N. Rao, D.A. Tryk, J. Photochem. Photobiol. C 1 (2000) 1–21.
[6] A. Fujishima, K. Honda, Nature 238 (1972) 37–38.
[7] A. Sanjuán, G. Aguirre, M. Álvaro, H. Garcíía, Appl. Catal. B Environ. 25 (2000) 257–265.
[8] H. Kotani, K. Ohkubo, S. Fukuzumi, Appl. Catal. B Environ. 77 (2008) 317–324.
[9] A. Sanjuán, G. Aguirre, M. Álvaro, H. Garcíía, J.C. Scaiano, Appl. Catal. B Environ. 15 (1998) 247–257.
[10] X. Wang, K. Maeda, A. Thomas, K. Takanabe, G. Xin, J.M. Carlsson, K. Domen, M. Antonietti, Nat. Mater. 8 (2009) 76–80.
[11] K. Takanabe, K. Kamata, X. Wang, M. Antonietti, J. Kubota, K. Domen, Phys. Chem. Chem. Phys. 12 (2010) 13020–13025.
[12] S.W. Hu, L.W. Yang, Y. Tian, X.L. Wei, J.W. Ding, J.X. Zhong, P.K. Chu, Appl. Catal. B Environ. 163 (2015) 611–622.
[13] L. Ge, C. Han, Appl. Catal. B Environ. 117–118 (2012) 268–274.
[14] H. Irie, Y. Watanabe, K. Hashimoto, J. Phys. Chem. B 107 (2003) 5483–5486.
[15] Z. Zou, J. Ye, K. Sayama, H. Arakawa, Nature 414 (2001) 625–627.
[16] I. Tsuji, H. Kato, H. Kobayashi, A. Kudo, J. Am. Chem. Soc. 126 (2004) 13406–13413.
[17] K. Maeda, K. Teramura, D. Lu, T. Takata, N. Saito, Y. Inoue, K. Domen, Nature 440 (2006) 295.
[18] H. Kato, A. Kudo, J. Phys. Chem. B 106 (2002) 5029–5034.
[19] K. Sayama, K. Mukasa, R. Abe, Y. Abe, H. Arakawa, Chem. Commun. (2001) 2416–2417.
[20] R. Asahi, T. Morikawa, T. Ohwaki, K. Aoki, Y. Taga, Science 293 (2001) 269–271.
[21] R. Abe, H. Takami, N. Murakami, B. Ohtani, J. Am. Chem. Soc. 130 (2008) 7780–7781.
[22] M. Yagi, S. Maruyama, K. Sone, K. Nagai, T. Norimatsu, J. Solid State Chem. 181 (2008) 175–182.
[23] S.S. Dunkle, R.J. Helmich, K.S. Suslick, J. Phys. Chem. C 113 (2009) 11980–11983.
[24] L. Zhang, J. Long, W. Pan, S. Zhou, J. Zhu, Y. Zhao, X. Wang, G. Cao, Mater. Chem. Phys. 136 (2012) 897–902.
[25] W. Zhao, Y. Guo, S. Wang, H. He, C. Sun, S. Yang, Appl. Catal. B Environ. 165 (2015) 335–343.
[26] B.M. Rajbongshi, S.K. Samdarshi, Appl. Catal. B Environ. 144 (2014) 435–441.
[27] R. Niishiro, S. Tanaka, A. Kudo, Appl. Catal. B Environ. 150–151 (2014) 187–196.
[28] J. Hirayama, R. Abe, Y.i Kamiya, Appl. Catal. B Environ. 144 (2014) 721–729.
[29] C.W. Tang, Appl. Phys. Lett. 48 (1986) 183–185.
[30] D. Schlettwein, N.R. Armstrong, J. Phys. Chem. 98 (1994) 11771–11779.
[31] S. Gunes, H. Neugebauer, N.S. Sariciftci, Chem. Rev. 107 (2007) 1324–1338.
[32] M. Hiramoto, H. Fujiwara, M. Yokoyama, Appl. Phys. Lett. 58 (1991) 1062–1064.
[33] P. Peumans, S. Uchida, S.R. Forrest, Nature 425 (2003) 158–162.
[34] T. Osasa, Y. Matsui, T. Matsumura, M. Matsumura, Sol. Energy Mater. Sol. Cells 90 (2006) 3136–3142.
[35] Y. Matsuo, Y. Sato, T. Niinomi, I. Soga, H. Tanaka, E. Nakamura, J. Am. Chem. Soc. 131 (2009) 16048–16050.
[36] Y. Zhen, N. Obata, Y. Matsuo, E. Nakamura, Chem. Asian J. 7 (2012) 2644–2649.
[37] T. Yamase, H. Harada, T. Ikawa, S. Ikeda, H. Shirakawa, Bull. Chem. Soc. Jpn. 54 (1981) 2817–2818.
[38] M. Aizawa, S. Watanabe, H. Shinohara, H. Shirakawa, J. Chem. Soc. Chem. Commun. (1985) 62–63.
[39] S. Yanagida, A. Kabumoto, K. Mizumoto, C. Pac, K. Yoshino, J. Chem. Soc. Chem. Commun. (1985) 474–475.
[40] T. Shibata, A. Kabumoto, T. Shiragami, O. Ishitani, C. Pac, S. Yanagida, J. Phys. Chem. 94 (1990) 2068–2076.
[41] S. Matsuoka, H. Fujii, T. Yamada, C. Pac, A. Ishida, S. Takamuku, M. Kusaba, N. Nakashima, S. Yanagida, J. Phys. Chem. 95 (1991) 5802–5808.
[42] K. Maruo, K. Yamada, Y. Wada, S. Yanagida, Bull. Chem. Soc. Jpn. 66 (1993) 1053–1064.
[43] T. Abe, K. Nagai, M. Kaneko, T. Okubo, K. Sekimoto, A. Tajiri, T. Norimatsu, ChemPhysChem 5 (2004) 716–720.
[44] T. Abe, K. Nagai, T. Ogiwara, S. Ogasawara, M. Kaneko, A. Tajiri, T. Norimatsu, J. Electroanal. Chem. 587 (2006) 127–132.
[45] T. Abe, S. Tobinai, N. Taira, J. Chiba, T. Itoh, K. Nagai, J. Phys. Chem. C 115 (2011) 7701–7705.
[46] T. Abe, J. Chiba, M. Ishidoya, K. Nagai, RSC Adv. 2 (2012) 7992–7996.

[47] T. Abe, N. Taira, Y. Tanno, Y. Kikuchi, K. Nagai, Chem. Commun. 50 (2014) 1950–1952.
[48] T. Abe, K. Nagai, K. Sekimoto, A. Tajiri, T. Norimatsu, Electrochem. Commun. 7 (2005) 1129–1132.
[49] T. Abe, K. Nagai, H. Ichinohe, T. Shibata, A. Tajiri, T. Norimatsu, J. Electroanal. Chem. 599 (2007) 65–71.
[50] T. Abe, S. Tobinai, K. Nagai, Jpn. J. Appl. Phys. 48 (2009) 021503.
[51] T. Abe, H. Ichinohe, S. Kakuta, K. Nagai, Jpn. J. Appl. Phys. 49 (2010) 015101.
[52] T. Abe, K. Nakamura, H. Ichinohe, K. Nagai, J. Mater. Sci. 47 (2012) 1071–1076.
[53] S. Zhang, R. Sakai, T. Abe, T. Iyoda, T. Norimatsu, K. Nagai, ACS Appl. Mater. Interfaces 3 (2011) 1902–1909.
[54] T. Abe, M. Ichikawa, T. Hikage, S. Kakuta, K. Nagai, Chem. Phys. Lett. 549 (2012) 77–81.
[55] K. Nagai, T. Abe, Koubunshi Ronbunshu, Jpn. J. Polym. Sci. Technol. 70 (2013) 459–475 (in Japanese).
[56] E. Lanzarini, M.R. Antognazza, M. Biso, A. Ansaldo, L. Laudato, P. Bruno, P. Metrangolo, G. Resnati, D. Ricci, G. Lanzani, J. Phys. Chem. C 116 (2012) 10944–10949.
[57] T. Abe, K. Nagai, S. Kabutomori, M. Kaneko, A. Tajiri, T. Norimatsu, Angew. Chem. Int. Ed. 45 (2006) 2778–2781.
[58] G. Tamizhmani, J.P. Dodelet, R. Côté, D. Gravel, Chem. Mater. 3 (1991) 1046–1053.
[59] F.-R. Fan, L.R. Faulkner, J. Am. Chem. Soc. 101 (1979) 4779–4787.
[60] K. Nagai, K. Morishita, H. Yoshida, T. Norimatsu, N. Miyanaga, Y. Izawa, T. Yamanaka, Synth. Met. 121 (2001) 1445–1446.
[61] K. Nagai, H. Yoshida, T. Norimatsu, N. Miyanaga, Y. Izawa, T. Yamanaka, Appl. Surf. Sci. 197–198 (2002) 808–813.
[62] K. Nagai, T. Abe, Y. Kaneyasu, Y. Yasuda, I. Kimishima, T. Iyoda, H. Imaya, ChemSusChem 4 (2011) 727–730.
[63] K. Nagai, Y. Yasuda, T. Iyoda, T. Abe, ACS Sustain. Chem. Eng. 1 (2013) 1033–1039.
[64] S. Zhang, P. Arunachalam, T. Abe, T. Iyoda, K. Nagai, J. Photochem. Photobiol. A Photochem. 224 (2012) 18–23.
[65] T. Yang, S. Zhang, M. Komura, T. Iyoda, K. Nagai, Jpn. J. Appl. Phys. 51 (2012) 070201.
[66] H. Kasai, H.S. Nalwa, H. Oikawa, S. Okada, H. Matsuda, N. Minami, A. Kakuta, K. Ono, A. Mutoh, H. Nakanishi, Jpn. J. Appl. Phys. 31 (1992) L1132–L1134.
[67] T. Tachikawa, R.H. Chung, A. Masuhara, H. Kasai, H. Oikawa, H. Nakanishi, M. Fujitsuka, T. Majima, J. Am. Chem. Soc. 128 (2006) 15944–15945.
[68] K. Baba, H. Kasai, K. Nishida, H. Nakanishi, Jpn. J. Appl. Phys. 50 (2011) 010202.
[69] V.L. Aksenov, M.V. Avdeev, E.A. Kyzyma, L. Rosta, M.V. Korobov, Crystallogr. Rep. 52 (2007) 479–482.
[70] H. Imahori, K. Mitamura, Y. Shibano, T. Umeyama, Y. Matano, K. Yoshida, S. Isoda, Y. Araki, O. Ito, J. Phys. Chem. B 110 (2006) 11399–11405.
[71] S. Kang, T. Umeyama, M. Ueda, Y. Matano, H. Hotta, K. Yoshida, S. Isoda, M. Shiro, H. Imahori, Adv. Mater. 18 (2006) 2549–2552.
[72] H. Imahori, M. Ueda, S. Kang, H. Hayashi, S. Hayashi, H. Kaji, S. Seki, A. Saeki, S. Tagawa, T. Umeyama, Y. Matano, K. Yoshida, S. Isoda, M. Shiro, N. Tkachenko, H. Lemmetyinen, Chem. Eur. J. 13 (2007) 10182–10193.
[73] H. Imahori, J. Mater. Chem. 17 (2007) 31–41.
[74] J.H. Zagall, Coord. Chem. Rev. 119 (1992) 89–136.
[75] Y. Ohkatsu, T. Tsuruta, Bull. Chem. Soc. Jpn. 51 (1978) 188–191.
[76] N. Takamiya, T. Yamaguchi, T. Iwatuki, S. Murai, Nippon Kagaku Kaishi (1977) 1775–1779 (in Japanese).
[77] N. Nemoto, T. Asakura, K. Tobita, Y. Ueno, K. Ikeda, N. Takamiya, J. Mol. Catal. 70 (1991) 151–158.
[78] H. Shirai, H. Tsuiki, E. Masuda, T. Koyama, K. Hanabusa, J. Phys. Chem. 95 (1991) 417–423.
[79] J.H. Zagal, M. Gulppi, A.C. Depretz, D. Lelievre, J. Porphyr. Phthalocyanine 3 (1999) 355–363.
[80] A.B. Sorokin, F. Quignard, R. Valentin, S. Mangematin, Appl. Catal. A 309 (2006) 162–168.
[81] A. Shaabani, E. Farhangi, A. Rahmati, Appl. Catal. A Gen. 338 (2008) 14–19.
[82] A. Kotronarou, M.R. Hoffmann, Environ. Sci. Technol. 25 (1991) 1153–1160.
[83] B.N. Achar, T.M. Mohan Kumar, K.S. Lokesh, J. Coord. Chem. 60 (2007) 1833–1846.
[84] A. Nisha, J. Janaki, V. Sridharan, G. Padma, M. Premila, T.S. Radhakrishnan, Thermochim. Acta 286 (1996) 17–24.
[85] A.L. Patterson, Phys. Rev. 56 (1934) 978–982.
[86] B. Böttger, U. Schindewolf, D. Möbius, J.L. Ávila, M.T. Martín, R. Rodríguez-Amaro, Langmuir 14 (1998) 5188–5194.